

EditTransfer++: Toward Faithful and Efficient Visual-Prompt-Guided Image Editing

Lan Chen, Qi Mao, *Member, IEEE*, Yiren Song, Yuchao Gu, Siwei Ma, *Fellow, IEEE*

Abstract—Visua-prompt-guided edit transfer aims to learn image transformations directly from example pairs, offering more precise and controllable editing than purely text-driven approaches. However, existing diffusion transformer-based methods often fail to faithfully reproduce the demonstrated edits due to structural mismatches between the task and the backbone, including a pretrained bias toward textual conditioning and inherent stochastic instability during sampling. To bridge this gap, we present EditTransfer++, a framework that combines progressively structured training with an efficient conditioning scheme to improve both visual prompt faithfulness and inference efficiency. We first mitigate textual dominance with a text-decoupled training strategy that removes text conditioning during fine-tuning, compelling the model to infer transformations solely from visual evidence while still supporting optional text guidance at inference. On top of this visually grounded model, a best–worst contrastive refinement mechanism reshapes the denoising trajectories to suppress unfaithful generations and improve consistency across random seeds. To alleviate the computational bottleneck of high-resolution in-context editing, we further introduce a condition compression and reuse strategy that reduces token redundancy and enables efficient generation of images with a 1024-pixel long edge. Extensive experiments on existing benchmarks and the proposed EditTransfer-Bench show that EditTransfer++ achieves state-of-the-art visual prompt faithfulness with substantially faster inference than prior methods, suggesting a promising direction for scalable prompt-guided image editing and broader visual in-context learning.

Index Terms—Image editing, diffusion models, visual prompt-guided edit transfer, in-context learning.

I. INTRODUCTION

IMAGE editing has rapidly advanced in recent years, with text-based image editing methods (TIE) [1]–[5] becoming the dominant paradigm due to their flexibility in specifying user intent through natural language. However, textual descriptions often fail to convey fine-grained transformations or compositional visual concepts, resulting in edits that deviate from the intended modification. To overcome the inherent ambiguity of text, recent works [6]–[12] have turned to *visual prompts*—paired examples consisting of a source and a target image that explicitly demonstrate the desired transformation. This paradigm, termed **Edit Transfer** [9], requires the model to faithfully apply the transformation illustrated in the visual

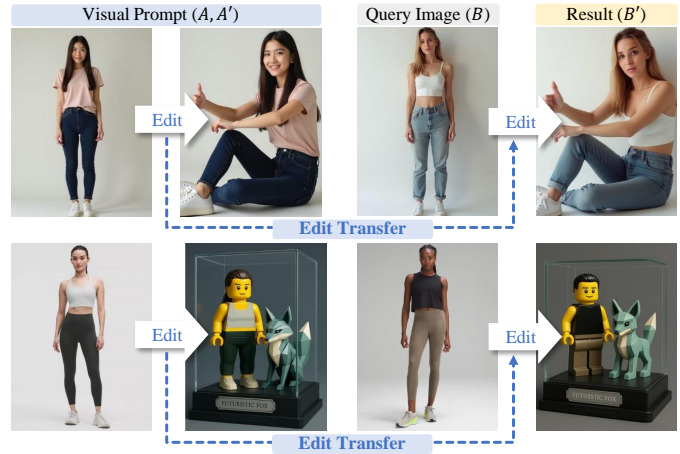


Fig. 1. **Illustration of the edit transfer task.** A visual prompt is defined as a pair of images (A, A') , where A' is an edited version of A . Given a query image B , the goal of edit transfer is to apply the transformation demonstrated by (A, A') to B , yielding an edited result B' .

prompt (A, A') to a new query image B , as shown in Fig. 1. Compared with textual instructions, visual prompts provide concrete and unambiguous guidance, making edit transfer a promising direction for controllable and faithful image editing.

Recent approaches [9]–[11], [13] increasingly build on DiT-based text-to-image (T2I) architectures [14], which offer several appealing properties: a unified tokenization scheme that permits seamless integration of additional images and the Multi-Modal Attention (MMA) [15] mechanism that naturally supports cross-condition interactions. These properties endow the DiT-based T2I models with in-context learning capabilities and inspire simplified edit-transfer frameworks such as VisualCloze [10] and RelationAdapter [11]. Nevertheless, *faithfully reproducing the transformation demonstrated in the visual prompt remains challenging*—especially for complex compositional edits such as coupling non-rigid motion with background changes, as illustrated in Fig. 2, where existing methods either miss parts of the pose change or fail to adapt the background consistently. These failures motivate a closer examination of why T2I backbones struggle with visual-prompt-guided edit transfer.

We identify two structural mismatches between T2I backbones and the requirements of the edit transfer task: (1) **Textual dominance**. T2I models are pretrained to prioritize textual conditioning, and retaining text input during fine-tuning [9]–[11] reinforces this bias. Consequently, cross-attention continues to favor textual tokens over visual ones, causing the model to associate visual effects with specific textual cues instead of learning the transformation conveyed by the visual prompt. (2) **Stochastic nature**. Diffusion-based sampling introduces

Lan Chen and Qi Mao are with the School of Information and Communication Engineering and the State Key Laboratory of Media Convergence and Communication, Communication University of China, Beijing 100024, China (E-mail: chenlaneva@mails.cuc.edu.cn, qimao@cuc.edu.cn) (Corresponding author: Qi Mao).

Yiren Song and Yuchao Gu are with ShowLab, National University of Singapore, 119077, Singapore (E-mail: yuchaogu@u.nus.edu, yiren@nus.edu.sg). Siwei Ma is with the State Key Laboratory of Multimedia Information Processing, School of Computer Science, Peking University, Beijing 100871, China (E-mail:swma@pku.edu.cn).



Fig. 2. **Edit transfer results and inference time.** Given a visual prompt and a query image, existing methods (a) EditTransfer [9], (b) VisualCloze [10], and (c) RelationAdapter [11] often fail to faithfully reproduce the demonstrated transformation and require long per-image inference time for 1024-long-edge outputs. Our (d) EditTransfer++ more closely follows the visual prompt while achieving much faster inference, as illustrated by the bar plots on the right.

inherently random denoising trajectories designed to promote output diversity. However, edit transfer requires deterministic reproduction of a specific transformation. Small variations in the initial noise are amplified during sampling, and the visual prompt alone cannot anchor the generation path, resulting in significant seed-induced variability and reduced adherence to the demonstrated transformation.

To address these challenges, we propose **EditTransfer++**, which refines the T2I backbone through a *progressively structured training procedure* designed to reduce textual bias and stabilize sampling behavior. We first encourage the model to rely directly on the visual prompt by removing textual conditioning during training, allowing it to learn the transformation from visual evidence alone. This **text-decoupled training** strengthens the influence of the visual prompt while preserving the backbone’s inherent ability to incorporate text at inference when needed. Building upon this visually grounded model, we introduce a **best–worst contrastive refinement** mechanism to further improve generation consistency. For each training instance, multiple outputs are sampled under different noise seeds and ranked according to their alignment with the visual prompt. The model is then guided to move away from the least faithful latent states and toward the most faithful ones, effectively reducing seed-induced variability and improving visual prompt adherence. Together, this progressively refined training procedure leads to substantially improved *faithfulness* to the demonstrated transformation and yields stable, consistent visual-prompt-guided edits.

While the progressive training procedure improves faithfulness, the overall scalability of EditTransfer++ is still limited by the in-context design, which concatenates all conditional images into a single token sequence. This leads to quadratic growth in computation and memory, making high-resolution generation prohibitively expensive. To improve efficiency and broaden applicability, we incorporate a *condition compression and reuse strategy* into our framework. This strategy reduces both sequence length and token computation by downsampling the conditional images and reusing their nearly invariant token features across inference steps. We systematically explore different compression configurations to identify the best balance between efficiency and performance. With the final configuration, EditTransfer++ is capable of generating images at a long-edge resolution of 1024 in an average of 16 seconds.

To thoroughly evaluate the effectiveness of EditTransfer++, we construct **EditTransfer-Bench**, a comprehensive benchmark designed to measure how well a model follows the transformation demonstrated in the visual prompt. It covers diverse editing scenarios spanning multiple edit types and visual effects (*e.g.*, pose changes, appearance adjustments, and style modifications), including both single-step and compositional edits. Using this benchmark, we perform extensive quantitative and qualitative evaluations. Our method consistently achieves higher faithfulness to the demonstrated transformation and offers significantly improved efficiency compared with existing approaches, as illustrated in Fig. 2.

The main contributions are summarized as follows:

- We introduce **EditTransfer++**, a framework that substantially improves visual-prompt faithfulness while offering significantly better computational efficiency.
- We design a progressively structured training procedure that integrates *text-decoupled training* with *best–worst contrastive refinement*, effectively reducing textual bias and seed-induced variability during sampling.
- We develop **EditTransfer-Bench**, a comprehensive benchmark covering diverse editing categories (*e.g.*, pose changes, appearance adjustments, and style modifications) across both single-step and compositional settings, and show through extensive quantitative and qualitative studies that EditTransfer++ achieves superior visual-prompt adherence and efficiency over existing methods.

II. RELATED WORK

A. Diffusion-Based Text-to-Image Models

Diffusion models such as DDPM [16] and DDIM [17] have become a standard paradigm for high-quality, controllable image generation, and have been widely adopted for text-conditioned synthesis and image editing [1], [3], [18]–[20]. Most diffusion-based T2I models initially adopt U-Net backbones [21], where spatial feature maps are progressively refined across scales. More recently, Transformer-based architectures such as DiT [14] have gained prominence. DiT tokenizes an image into patch embeddings and represents it as a sequence of visual tokens processed by full self-attention. This *unified tokenization* naturally accommodates multiple images concatenated along the token dimension, while MMA allows tokens from different conditions (*e.g.*, text,

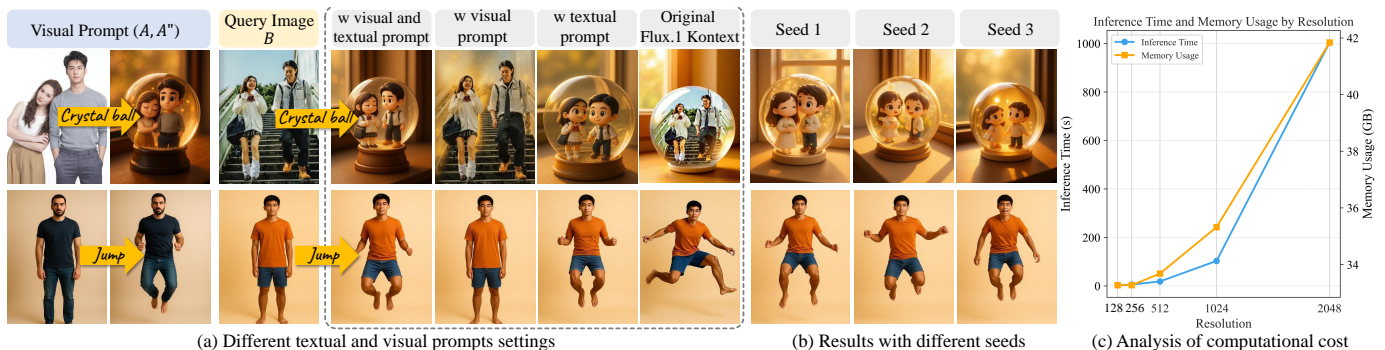


Fig. 3. **Limitations of naive DiT-based in-context design for edit transfer.** (a) Training with paired text–image supervision causes the model to over-associate specific visual effects with textual cues, so removing the text greatly weakens the influence of the visual prompt. (b) Even with the same visual prompt and text, the fine-tuned model produces divergent outputs under different random seeds, revealing low visual-prompt faithfulness. (c) Concatenating all images into a single long token sequence makes inference time and memory usage grow rapidly with resolution, creating a major efficiency bottleneck.

reference images, or visual prompts) to attend to each other and exchange information.

Thanks to these properties, DiT-based models exhibit strong *in-context conditioning* ability [22]: additional visual examples can be injected as extra token sequences and treated as context during generation. Such capability has been leveraged in controllable generation [23]–[26], instruction-guided editing [4], [27], and, more recently, visual-prompt-guided edit transfer [9]–[11], [13]. However, because DiT backbones are pre-trained with text-dominant T2I objectives and rely on stochastic sampling, naively adapting them to edit transfer by concatenating multiple images still suffers from textual bias, seed-induced inconsistency, and substantial computational overhead, which motivates the design of our tailored training and conditioning scheme.

B. Guided Image Editing with Textual and Visual Cues

Guided image editing methods can be broadly categorized according to the type of guidance they use, most notably *textual descriptions* and *visual references*. Text-guided approaches provide flexible, high-level control through natural language, whereas visual-guided approaches supply concrete examples that capture details difficult to describe with text alone. We briefly review both families and highlight their limitations in expressing complex transformations, which motivates our visual-prompt-guided formulation.

Text-guided image editing [1]–[3], [28]–[31], [31], [32] rely on natural language to specify the desired modification. Training-free strategies based on attention manipulation or injection [1], [2], [28]–[30] intervene in the cross- or self-attention maps of diffusion models, enabling diverse edits such as appearance changes, object replacement, and non-rigid transformations. However, they typically require detailed prompts describing both the original scene and the intended edit, which increases prompt engineering burden and may disperse attention over irrelevant tokens, leading to coarse or incomplete edits. To alleviate prompt complexity, instruction-based approaches [3], [33], [34] train diffusion models on large-scale datasets of image–instruction pairs, allowing users to specify edits via natural language commands. Despite these advances, a fundamental gap remains between textual

descriptions and visual content: *language alone often struggles to encode fine-grained visual semantics, such as subtle pose changes, precise spatial relations, or detailed textures*. Consequently, even well-crafted prompts do not always yield edits that faithfully realize the intended visual transformation. **Visual-guided image editing** incorporates an auxiliary image as a guidance signal to compensate for what text cannot easily express. Early work on style transfer [35], [36] focuses on propagating global artistic characteristics from the guidance image to the target. Subsequent approaches [37]–[40] establish semantic correspondences between images to transfer appearance across aligned regions, while more recent methods [41]–[47] enable localized control, such as copying hair color, clothing patterns, or object textures from the guidance image to specific target regions. Although effective for fine-grained appearance and style transfer, these techniques largely remain limited to low- or mid-level visual attributes and generally do not model *high-level transformations* such as complex non-rigid motions or action changes.

In summary, text-guided editing offers semantic flexibility but suffers from ambiguity and limited control over fine-grained details, while visual-guided editing provides precise appearance cues but is restricted in the types of edits it can express. These limitations motivate the use of *visual prompts* that explicitly demonstrate a source-to-target transformation, which we formalize as the **Edit Transfer** task [9] and further discuss in the next subsection.

C. Visual-Prompt-Guided Edit Transfer

Inspired by the in-context learning ability of large language models (LLMs), which can learn behaviors from input–output pairs, recent works extend this idea to vision by using paired examples as *visual prompts*. In this setting, a visual prompt consists of a source and a target image that demonstrate a specific transformation, and the goal is to transfer this transformation to a new query image—a task referred to as *edit transfer* [9].

Early visual in-context learning methods leverage inpainting models [6], [48], [49] and masked image modeling [50], [51], mainly focusing on dense prediction and low-level understanding tasks. ImageBrush [8] first extends this paradigm to image editing: it proposes a visual-prompt-guided framework that

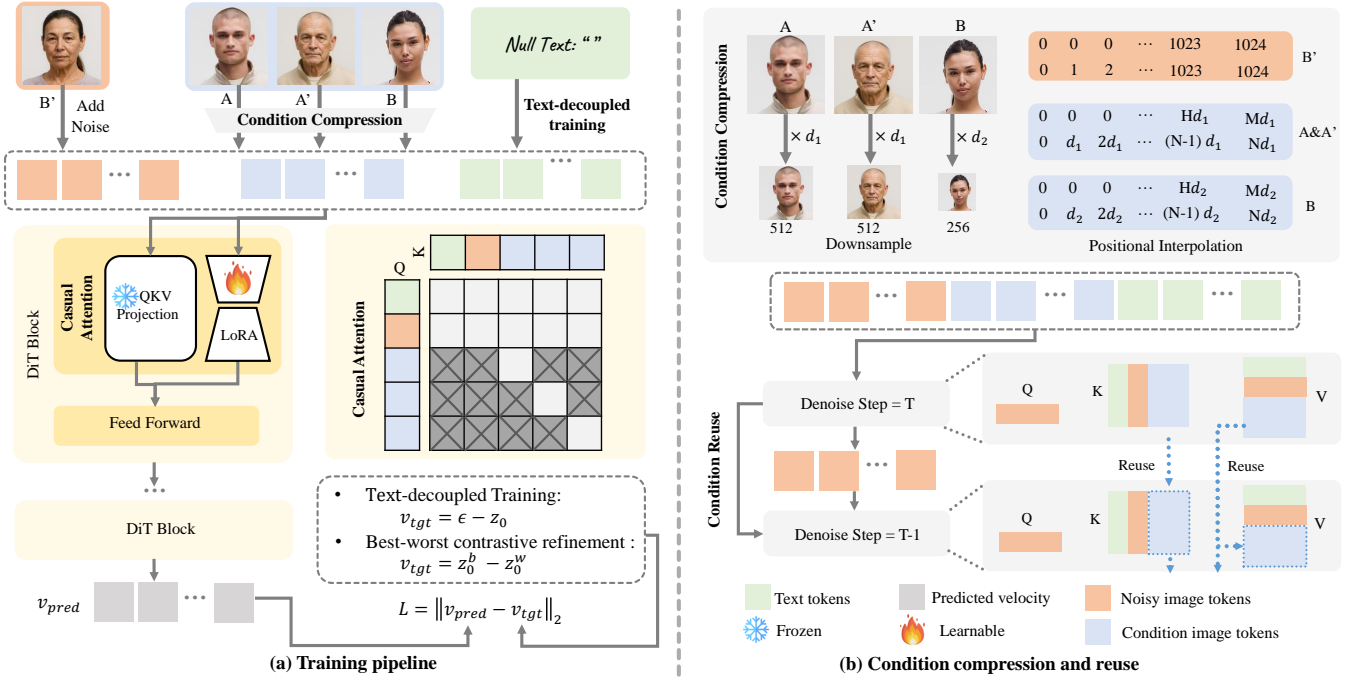


Fig. 4. **Framework of EditTransfer++.** (a) *Training pipeline.* During training, the text branch is fed with null text to enable text-decoupled learning, while the conditional images (A, A', B) are downsampled for condition compression. The full token sequence (A, A', B, B') is then processed by the DiT backbone, where causal attention ensures that the conditional tokens (A, A', B) remain unaffected by the noisy target tokens. The network predicts the velocity of B' , which is used to compute the loss under the progressive training procedure (text-decoupled training followed by best-worst contrastive refinement). (b) *Condition compression and reuse.* For efficiency, we fix the output resolution to a 1024-pixel long edge, and apply condition compression by downsampling (A, A') with ratio d_1 and B with ratio d_2 . To maintain spatial alignment between B' and the conditional images, token positions are remapped to the original resolution according to the downsampling ratios. During inference, conditional features are computed once, cached, and reused across subsequent timesteps.

injects prompt features into the cross-attention layers of a U-Net-based diffusion model via an auxiliary network, thereby broadening the scope of visual in-context learning beyond analysis tasks.

Building on more powerful diffusion transformer architectures, recent works adopt a simpler token-based conditioning strategy. EditTransfer [9] concatenates the visual tokens of the prompt and query images, enabling the backbone to directly attend to visual guidance during generation; with only dozens of training samples, it can adapt a pretrained text-to-image model for visual-prompt-guided editing and significantly improve complex non-rigid transformations over purely text- or reference-guided methods. To further enhance generalization, VisualCloze [10] constructs a large-scale dataset of densely related visual tasks, where each image is annotated under multiple task formulations to encourage the learning of shared transformation patterns. Instead of relying solely on token concatenation as in EditTransfer and VisualCloze, Relation-Adapter [11] introduces a lightweight adapter branch for visual prompt guidance and proposes a more diverse dataset covering a broader range of editing types.

Despite these advances, existing visual-prompt-guided methods still exhibit limited faithfulness to the demonstrated transformation, sensitivity to sampling randomness, and high computational cost when multiple images are concatenated into a single long token sequence. In contrast, our EditTransfer++ framework tackles these issues through a progressively structured training procedure and a condition compression and reuse scheme, jointly improving visual prompt adherence and

inference efficiency.

III. METHODOLOGY

In this section, we present the methodology of **EditTransfer++**, which enhances faithfulness and efficiency in visual-prompt-guided image editing. We first revisit the DiT-based T2I backbone in Section III-A and analyze the limitations of naïve in-context learning strategies for edit transfer in Section III-B. Building on these observations, we introduce a progressive training procedure (detailed in Section III-C), comprising text-decoupled training and best-worst contrastive refinement, to gradually reduce textual bias and sampling instability. To further enhance practical applicability, we incorporate a condition compression and reuse strategy in Section III-D, which reduces token length and redundant computation.

A. Preliminary: DiT-based T2I model

DiT-based T2I models (e.g., FLUX [52]) adopt token-based representations and Transformer architectures similar to LLMs, enabling in-context generation. In their standard design, noisy image tokens $z \in \mathbb{R}^{N \times d}$ are processed jointly with textual tokens $c_T \in \mathbb{R}^{M \times d}$ across Transformer-based DiT blocks. Each DiT block incorporates the MMA module to fuse noisy tokens z and text tokens c_T . This flexible, expandable token-sequence design allows the introduction of additional visual conditions. For example, in the TIE model FLUX.1 Kontext [5], the source image is encoded into visual tokens c_V , which are directly appended to the input sequence.

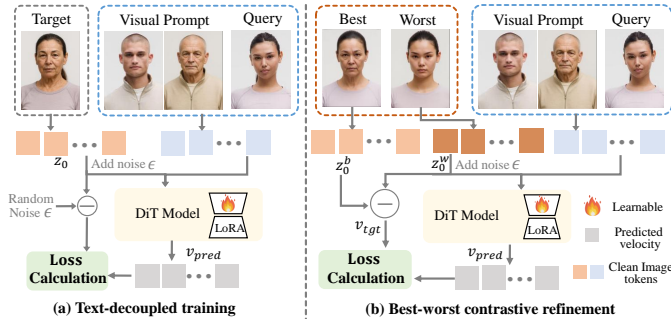


Fig. 5. **Detailed illustration of the progressive training procedure.** (a) In text-decoupled training, the LoRA modules are first fine-tuned using the standard velocity loss in Eq. (4). (b) In best-worst contrastive refinement, we construct a best-worst contrastive dataset and further update the LoRA with the contrastive objective in Eq. (8) to improve generation consistency.

The resulting token sequence $[c_T; z; c_V]$ is then projected into query (Q), key (K), and value (V) matrices and processed by the MMA module to guide the edited output:

$$\text{MMA}([c_T; z; c_V]) = \text{softmax}\left(\frac{QK^T}{\sqrt{d}}\right)V. \quad (1)$$

This bidirectional attention mechanism enables interactions among noisy tokens, visual condition tokens, and textual condition tokens, forming the foundation of DiT-based edit transfer methods.

Based on this architecture, DiT-based T2I models are typically trained under a rectified-flow objective [53], [54] to model a continuous transport between a noise distribution $z_1 \sim \pi_1$ and a data distribution $z_0 \sim \pi_0$. This is achieved by parameterizing an ODE, $\frac{dz_t}{dt} = v_\theta(z_t, t)$, where v_θ is instantiated by the DiT network to predict the velocity of the latent path. During training, the forward process is implemented by:

$$z_t = (1 - t)z_0 + tz_1, \quad t \in [0, 1], \quad (2)$$

whose time derivative yields the ground-truth velocity:

$$\frac{dz_t}{dt} = z_1 - z_0, \quad t \in [0, 1]. \quad (3)$$

The model is optimized to regress this velocity via:

$$\theta = \arg \min_{\theta} \mathbb{E}[\|(z_1 - z_0) - v_\theta(z_t, t)\|^2]. \quad (4)$$

While fine-tuning typically uses the same reconstruction objective as in Eq. (4) on a supervised dataset, the formulation is flexible and can be adapted to specific goals.

B. Motivation and Analysis

To empirically examine the limitations discussed in Section I, we conduct a naïve LoRA fine-tuning experiment on FLUX.1 Kontext [5] using standard supervised training with both text and visual prompts. Each training sample consists of a visual prompt (A, A'), a query image B , a target image B' , and a textual instruction P .

Observation 1 (Textual dominance). As shown in Fig. 3(a), the fine-tuned model behaves well when both text and visual prompts are provided. However, once the textual instruction is removed, it can no longer follow the transformation indicated by (A, A'), while text-only editing still produces



Fig. 6. **Data samples in Relation252K and EditTransfer-Bench.** (a) In the Relation252K [11] test split, each editing type exhibits nearly identical visual effects across samples, offering limited diversity for evaluating edit generalization. (b) In contrast, EditTransfer-Bench introduces both diverse editing types and varied visual outcomes, enabling a more comprehensive evaluation of edit transfer capabilities.

reasonable results. This suggests that the model largely binds the visual effects to textual cues and under-utilizes the visual prompt, motivating our text-decoupled training strategy in Section III-C.

Observation 2 (Stochastic nature). Even when both text and visual prompts are fixed, the model generates noticeably different outputs under different random seeds, as illustrated in Fig. 3(b). Such seed sensitivity reflects the inherent stochasticity of diffusion sampling and leads to low visual-prompt faithfulness in edit transfer, which our best-worst contrastive refinement is designed to mitigate.

Beyond faithfulness limitations, the naïve in-context design also suffers from efficiency bottlenecks. As discussed in Section III-A, DiT-based models incorporate visual guidance by concatenating all condition tokens into a single input sequence. For edit transfer, four images—an example pair, a query image, and a target image—must be jointly encoded, so if each image is tokenized into L tokens, the sequence length becomes $4L$ and the attention complexity scales as $\mathcal{O}((4L)^2)$. The empirical measurements in Fig. 3(c) show that both memory usage and inference time grow rapidly with image resolution, motivating the condition compression and reuse scheme introduced in Section III-D.

C. Progressive Training Procedure

Based on the above analysis, we introduce a progressively structured training procedure, including *text-decoupled training* and the *best-worst contrastive refinement* to enhance visual-prompt faithfulness.

Text-decoupled training. As discussed in Section III-B, naïvely fine-tuned models tend to overfit textual instructions

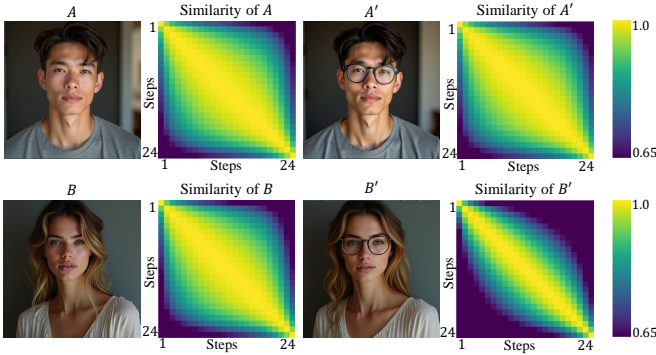


Fig. 7. **Feature similarity across timesteps for each image.** We extract intermediate features of each image (A, A', B, B') at every timestep and compute pairwise similarities over time, visualized as heatmaps. Higher similarity is shown in yellow and lower similarity in dark blue. The conditional images (A, A', B) exhibit highly stable features across timesteps, whereas the target B' changes significantly, supporting our design of reusing condition features during inference.

and exhibit weak responsiveness to visual prompts. To address this bias, we remove textual conditioning during training by feeding null input to the text branch (see Fig. 4(a)), thereby eliminating linguistic supervision. Under this constraint, the model is forced to learn the visual relations among the visual prompt (A, A'), the source image B , and the target image B' . This simple but effective strategy enhances the influence of visual prompts while preserving the backbone’s inherent text-guided editing capability. At inference, the model remains compatible with visual-only, text-only, or combined guidance, offering flexible control as shown in Section IV-F.

Best-worst contrastive refinement. Although text-decoupled training improves visual alignment, the results still vary significantly across different sampling seeds. To mitigate this, we introduce an offline refinement stage built upon the previously fine-tuned model. For each training sample, we generate R candidate outputs using different random seeds and rank them according to the CLIP direction score [55], supplemented by manual verification. The sample that best preserves the demonstrated transformation is designated as the *best* image I^b , while the most deviating one is selected as the *worst* image I^w , forming a best-worst contrastive pair. Unlike standard fine-tuning, which regresses toward ground-truth data as in Eq. (4), our refinement objective actively steers the model away from undesirable latent trajectories and toward those that align with the visual prompt. Although the flow-matching objective in Eq. (4) is derived from the continuous formulation in Eq. (2), the generation process is ultimately carried out through discrete sampling. To align with the model’s inference dynamics, we ground it in the Euler-based discretization used during sampling:

$$z_{t_{i-1}} = z_{t_i} + (t_{i-1} - t_i)v_{\theta}(z_{t_i}, t_i), \quad (5)$$

where the sampling process contains discrete T timesteps, $t = \{t_T, \dots, t_0\}$ and $i \in \{T, \dots, 1\}$. Based on this discrete formulation, we define a contrastive velocity v_{cts} that pushes z_t toward the best sample z^b and away from the worst sample z^w :

$$v_{cts} = \frac{z^b - z_t^w}{\lambda}, \quad (6)$$

TABLE I
QUANTITATIVE COMPARISONS OF EDIT TRANSFER METHODS. BOLD INDICATES THE BEST RESULT.

Method	Fidelity		Alignment		Consistency	
	DS↓	GPT-F↑	CDS↑	GPT-A↑	SR↑	Var↓
Relation252K: Image Editing						
ET [9]	0.202	6.751	0.318	7.209	0.672	3.39e-3
VC [10]	0.217	7.105	0.236	6.156	0.155	4.17e-3
RA [11]	0.177	9.128	0.363	8.991	0.889	1.12e-3
Ours	0.259	8.911	0.401	9.041	0.949	1.11e-3
Relation252K: Low-Level						
ET [9]	0.212	5.883	0.189	4.202	0.167	2.90e-3
VC [10]	0.253	6.824	0.333	6.201	0.354	1.39e-3
RA [11]	0.202	7.158	0.257	5.753	0.451	8.12e-4
Ours	0.260	5.992	0.245	6.889	0.437	7.26e-4
Relation252K: Customized Generation						
ET [9]	0.232	6.200	0.298	6.812	0.401	4.09e-3
VC [10]	0.297	6.713	0.264	7.489	0.378	3.81e-3
RA [11]	0.279	8.505	0.384	8.495	0.739	1.27e-3
Ours	0.337	8.670	0.389	8.826	0.744	1.20e-3
EditTransfer-Bench						
ET [9]	0.157	6.454	0.148	6.122	0.230	5.70e-3
VC [10]	0.159	7.243	0.240	6.322	0.322	4.40e-3
RA [11]	0.159	8.925	0.229	7.580	0.347	3.68e-3
Ours	0.169	8.631	0.292	8.152	0.397	2.37e-3

TABLE II
COMPARISON OF INFERENCE TIME AND MEMORY CONSUMPTION ACROSS METHODS.

Method	ET [9]	VC [10]	RA [11]	PE [12]	Ours
Time(s)	75.05	70.91	29.93	28.19	15.93
Memory(GB)	39.84	37.81	40.54	33.95	41.55

where the time-dependent term $t_{i-1} - t_i$ is replaced with the scaling constant λ . By applying identical noise to both z_0^b and z_0^w under the linear interpolation in Eq. (2), Eq. (6) simplifies to:

$$v_{cts} = \frac{z_0^b - z_0^w}{\lambda}. \quad (7)$$

The refinement stage then minimizes the discrepancy between the model velocity and this contrastive target:

$$\arg \min_{\theta} \mathbb{E} \left[\left\| \left(\frac{z_0^b - z_0^w}{\lambda} \right) - v_{\theta}(z_t, t) \right\|^2 \right], \quad (8)$$

where θ denotes the same LoRA parameters optimized during the text-decoupled training. After this contrastive refinement, the model exhibits improved faithfulness to visual prompts. This overall progressive training procedure is illustrated in Fig. 5.

D. Condition Compression and Reuse

To improve efficiency and broaden applicability, we integrate a condition compression and reuse strategy, effectively reducing both the sequence length and the attention computation cost.

Condition compression. Let the conditional images (A, A', B) have resolution $H \times W$, and the target output B' be $M \times N$. We downsample the visual prompt (A, A') to

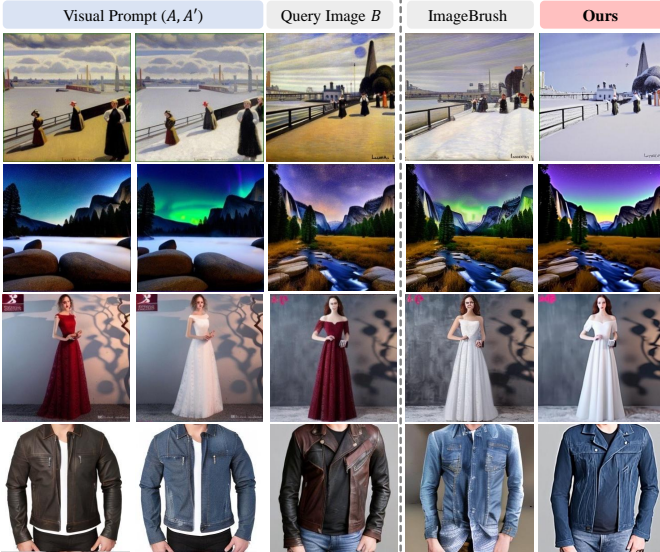


Fig. 8. **Qualitative comparisons with ImageBrush [8].** Since ImageBrush is not open-source, we use the examples provided in its original paper for comparison. Given the same visual prompts and query images, our method not only follows the demonstrated transformation more faithfully, but also better preserves the identity and structure of the query image.

$\frac{M}{2} \times \frac{N}{2}$ and the query image B to $\frac{M}{4} \times \frac{N}{4}$. The corresponding downsampling ratios d_1 for (A, A') and d_2 for B are:

$$d_1 = \frac{H}{M/2}, \quad d_2 = \frac{H}{M/4}. \quad (9)$$

We justify this choice in Section IV-E through an empirical study of different configurations, identifying the best trade-off between efficiency and editing quality. This simple adjustment reduces the sequence length by nearly 61% while preserving editing quality. To maintain spatial correspondence among (A, A', B, B') after compression, we apply positional interpolation. For a token at position (i, j) in the resized conditional image, its original position (P_i, P_j) is computed as:

$$P_i = i \times d_*, \quad P_j = j \times d_*, \quad d_* \in \{d_1, d_2\}. \quad (10)$$

This mapping preserves alignment within the compressed token sequence.

Condition reuse. While the conditional images (A, A', B) remain clean throughout the denoising process, the naive fine-tuning pipeline re-encodes them at every timestep, introducing redundant computation. As shown in Fig. 7, the pairwise feature similarity across timesteps is consistently high for (A, A', B) , whereas it changes for B' , indicating that conditional features are temporally stable. To exploit this, we adopt causal attention to further isolate the interference from evolving noisy and text tokens. During attention calculation, (A, A', B) tokens are restricted to attend only to themselves, as illustrated in Fig. 4(a). The casual attention enables a lightweight KV-cache mechanism during inference: condition features of (A, A', B) are computed once and reused across timesteps, as shown in Fig. 4(c). The design reduces inference time significantly with minimal memory overhead, enhancing the practicality of EditTransfer++ for high-resolution generation.

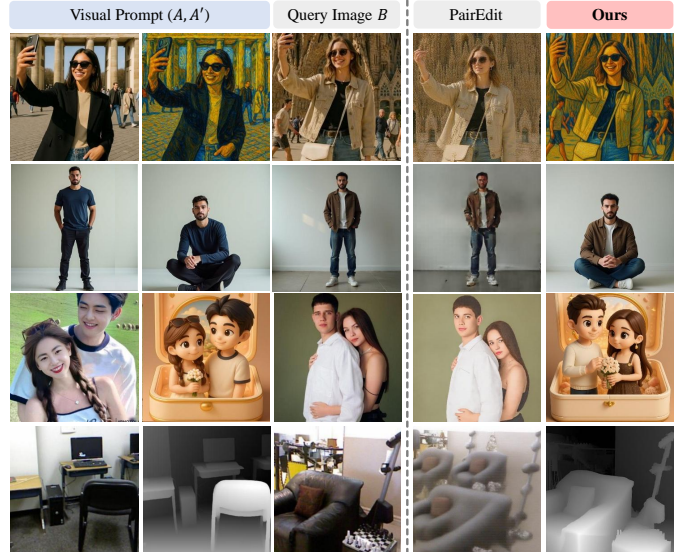


Fig. 9. **Qualitative comparisons with PairEdit [12].** We compare our method with PairEdit on image editing, customization, and low-level understanding tasks. Although PairEdit requires training a separate LoRA for each semantic variation, it often produces only subtle changes, whereas our method achieves stronger transformations that better follow the visual prompt.

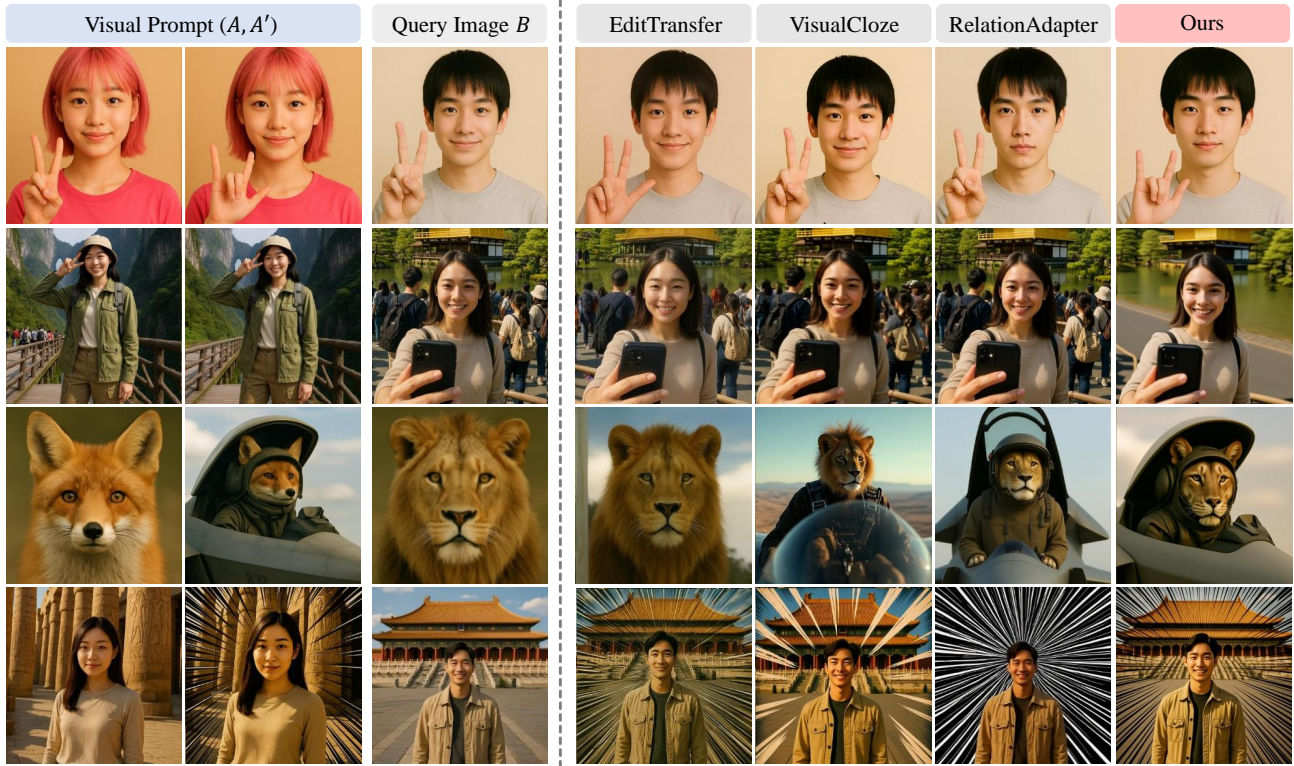
IV. EXPERIMENTS

A. Implementation Details

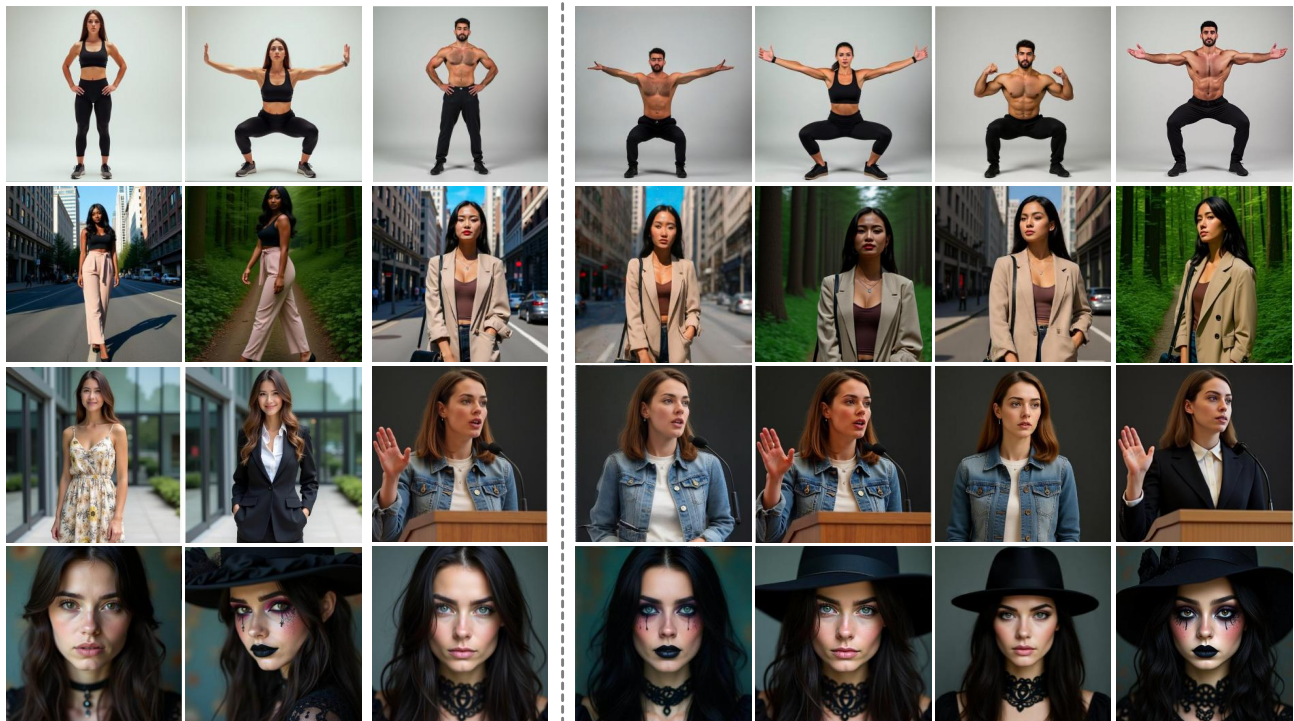
We initialize our model from FLUX.1 Kontext [5]. Following the 3D RoPE embedding in FLUX.1 Kontext, each conditional image is assigned a constant offset to separate context tokens from target tokens. Specifically, token positions are represented as triplets (k, i, j) , where $(0, i, j)$ is used for the target B' , $(1, i, j)$ for the query image B , and $(2, i, j)$ for the visual prompt (A, A') , with (i, j) denoting spatial coordinates. The scaling constant in Eq. (8) is set to 0.2. We fine-tune the model using LoRA with rank 128 and a learning rate of $1e-4$. Training is conducted on two H20 GPUs with an accumulated batch size of 4, using the AdamW optimizer [56] and bfloat16 mixed precision. The longer side of the target image B' is fixed at 1024 pixels. We train for 125,000 iterations on the training split of the Relation252K dataset [11].

B. Benchmarks

We evaluate our method on both the test split of Relation252K [11] and our constructed EditTransfer-Bench. The Relation252K [11] test split spans image editing, image customization, and low-level understanding. Its editing subset, however, exhibits limited diversity, with each editing type appearing in nearly fixed visual forms across the dataset. For example, as shown in Fig. 6(a), the “raising arms” edits remain identical throughout the dataset. This reduces the benchmark’s capacity to faithfully assess edit transfer generalization, particularly under diverse visual realizations of the same editing type. To address this limitation, we construct EditTransfer-Bench, a benchmark focused on image editing and designed to systematically evaluate model performance on diverse edit transfer tasks. Diversity is reflected in two aspects: (1) a wide variety of editing types, and (2) multiple distinct



(a) Results on Relation252K test split



(b) Results on EditTransfer-Bench

Fig. 10. **Qualitative comparisons with baselines on Relation252K and EditTransfer-Bench.** For each example, given a visual prompt (A, A') and a query image B , we compare the results of EditTransfer [9], VisualCloze [10], RelationAdapter [11], and our EditTransfer++. (a) Results on the Relation252K test split [11]. (b) Results on the proposed EditTransfer-Bench. Across diverse editing types and difficulty levels, our method more faithfully transfers the demonstrated transformation while better preserving the query image content.

visual realizations within each type. As illustrated in Fig. 6(b), EditTransfer-Bench consists of four primary editing categories, covering both single-edit and compositional-edit scenarios:

- **Non-rigid editing** focuses on complex motion patterns with high variability.

- **Style transfer** targets uncommon styles constructed using community-released LoRAs.
- **Background change** applies edits primarily to the background rather than the main subjects, a setting rarely seen in the training data.

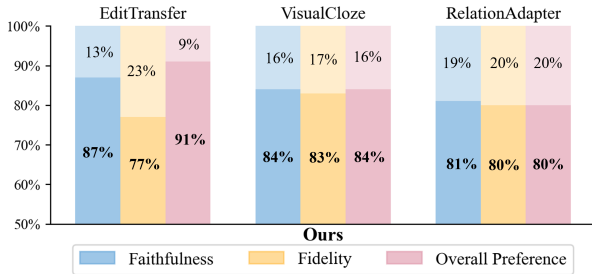


Fig. 11. **User study results.** Bars report the proportion of participants who preferred EditTransfer++ over each baseline (EditTransfer [9], VisualCloze [10], RelationAdapter [11]) in terms of faithfulness, fidelity, and overall preference. Across all three criteria, the majority of users favor our method.

- **Appearance transfer** emphasizes diverse local appearance modifications, such as adding glasses or changing clothing color.

These four categories and their combinations form a systematic benchmark to evaluate the model’s generalization.

C. Evaluation Metrics

We quantitatively evaluate our proposed method against baseline models using automatic metrics, large vision-language model (VLM) scores, and human evaluations.

Automatic metrics. Our automatic evaluation covers three aspects of the edit transfer behavior: *editing fidelity to the query image*, *visual-prompt faithfulness*, and *inference efficiency*. (1) *Editing fidelity to the query image.* Since edit transfer is instantiated as an image editing task, a reasonable edit should preserve content that is not intended to change (e.g., identity, global structure, and background context). To measure this, we compute the DINO-ViT self-similarity distance (DS) [57] between the query image B and the generated output B' . (2) *Visual-prompt faithfulness.* We characterize faithfulness to the visual prompt along two dimensions: (a) **Alignment with the visual prompt.** To evaluate whether the applied edit matches the transformation demonstrated by the visual prompt, we follow CLIP directional similarity [55] and compute the CLIP Direction Score (CDS) using CLIP ViT-L/14, which measures how well the editing direction of (B, B') aligns with that of (A, A') . (b) **Consistency across seeds.** Beyond aligning with the visual prompt on average, a faithful edit transfer model should reproduce the same transformation consistently under different random seeds. To assess this consistency, we measure the variance of CDS across generations (Var), where lower values indicate more stable behavior with respect to the intended editing direction. (3) *Inference efficiency.* For efficiency, we report inference time and peak GPU memory usage for each method.

VLM scores. To further assess editing quality from a human-centered perspective, we employ the VLM GPT-4o [58] to provide three metrics: (1) *GPT-F*, assessing the fidelity between the query image B and the output B' . (2) *GPT-A*, evaluating the alignment of the intended transformation between the visual prompt (A, A') and (B, B') ; and (3) *Success Rate*, estimating how consistently the model applies the intended transformation across different random seeds. Following the protocol in RelationAdapter [11], GPT-F and GPT-A are

TABLE III
QUANTITATIVE RESULTS OF ABLATION STUDY.

Method	DS↓	CDS↑	Var↓	Time(s)↓	Mem(GB)↓
Relation252K					
M_b : Base model	0.246	0.370	9.10e-3	72.14	39.00
M_1 : M_b + TD	0.232	0.374	3.54e-3	72.14	39.00
M_2 : M_1 + RF	0.247	0.379	2.43e-3	22.56	38.29
M_3 : M_2 + DS	0.249	0.375	1.09e-3	16.71	43.23
M_4 : M_3 + RU	0.268	0.376	1.02e-3	16.71	43.23
EditTransfer-Bench					
M_b : Base model	0.171	0.287	3.02e-3	67.04	37.62
M_1 : M_b + TD	0.184	0.311	3.81e-3	17.39	61.07
M_2 : M_1 + RF	0.167	0.304	3.07e-3	20.60	36.68
M_3 : M_2 + DS	0.173	0.288	2.17e-3	15.15	39.88
M_4 : M_3 + RU	0.169	0.292	2.37e-3	15.15	39.88

scored on a 0–10 scale, where higher scores indicate better performance. The success decision is binary, and we report the average success rate across multiple generations.

User study. To further evaluate the effectiveness of our method, we conduct a user study comparing it with existing approaches. In each questionnaire, participants are shown the visual prompt (A, A') , the query image B , and two output images: one generated by EditTransfer++ and the other by a baseline method. Participants are asked to answer the following questions:

- **Fidelity with the query image:** Which result better preserves consistency with the source image B ?
- **Alignment with visual prompt:** Which result better aligns with the demonstrated transformation from A to A' ?
- **Overall Quality:** Which image do you prefer overall?

D. Comparisons with State-of-the-art Methods

Baselines. We compare EditTransfer++ with representative visual prompt-guided editing methods and a related pairwise editing method:

- **U-Net-based visual prompt editing.** ImageBrush [8] is a U-Net-based method that first broadened visual in-context learning from low-level understanding tasks to image editing. It injects visual-prompt features into the cross-attention layers of a diffusion U-Net. Since its implementation and training code are not publicly released, we refer to the qualitative results reported in the original paper for comparison.
- **DiT-based edit transfer methods.** EditTransfer (ET) [9] is the first work to exploit the in-context learning ability of DiT-based models for edit transfer, primarily targeting non-rigid edits. Because the original model is trained on a small-scale dataset, we retrain it on Relation252K [11] for a fair comparison. VisualCloze (VC) [10] formulates edit transfer as a masked prediction/inpainting problem on a large-scale multi-task dataset. RelationAdapter (RA) [11] introduces a lightweight adapter branch to fuse visual prompts with DiT features.

TABLE IV
ABLATION STUDY ON THE DOWNSAMPLING RATIOS.

(A, A')	1024	512	256	512	256
(B)	1024	512	512	256	256
Relation252K					
DS ↓	0.232	0.250	0.246	0.247	0.246
CDS ↑	0.363	0.362	0.340	0.360	0.350
Time(s) ↓	72.14	26.02	19.88	22.56	17.45
Memory(GB) ↓	39.00	38.38	38.25	38.29	37.64
EditTransfer-Bench					
DS ↓	0.165	0.171	0.172	0.173	0.175
CDS ↑	0.240	0.304	0.295	0.298	0.291
Time(s) ↓	67.04	29.74	18.86	20.60	15.50
Memory(GB) ↓	37.62	36.90	36.64	36.68	36.66

- **Pairwise editing with learned variations.** PairEdit (PE) [12] learns a semantic variation from a set of source–target pairs and applies it to new inputs. This setting is different from our visual-prompt–guided edit transfer, which directly follows the specific transformation shown in a single example pair. Therefore, we include PE only in qualitative comparisons.

Editing fidelity to the query image. We first analyze how well each method preserves content in the query image B that is not meant to change. As shown in the first row of Fig. 10(b), VisualCloze [10] tends to overfit the visual prompt and fails to maintain subject identity in B , producing an edited image B' whose global appearance drifts toward the prompt. Similarly, in the fourth row of Fig. 8, ImageBrush [8] struggles to preserve fine-grained jacket textures. In contrast, EditTransfer++ adapts the strength of the edit according to the demonstrated transformation, preserving the subject’s shape, pose, and local appearance in B when these factors are not directly involved in the edit. Quantitatively, our method maintains competitive DS and achieves a strong VLM-based GPT-F score, while user preferences in Fig. 11 further indicate that edits produced by EditTransfer++ are more often judged as faithful to the query image.

Visual-prompt faithfulness. We next evaluate how faithfully each method follows the transformation demonstrated by the visual prompt (A, A') , both in terms of alignment and consistency.

Alignment. As illustrated in the first row of Fig. 10(a), EditTransfer [9] often fails to apply the intended pose change, leaving the gesture unchanged. In the second row, VisualCloze [10] and RelationAdapter [11] partially capture the “animal airforce” concept, but their layouts and fine-grained appearance deviate noticeably from the visual prompt. Moreover, Fig. 10(b) shows that when faced with compositional edits, existing DiT-based methods tend to complete only one of the required edits, even when full text guidance is provided. For PairEdit [12], it performs well on human facial appearance editing but struggles with low-level tasks, non-rigid edits, and customized generation, as illustrated in Fig. 9. In contrast, EditTransfer++ can handle both seen and diverse unseen cases, including single and compositional edits, while closely

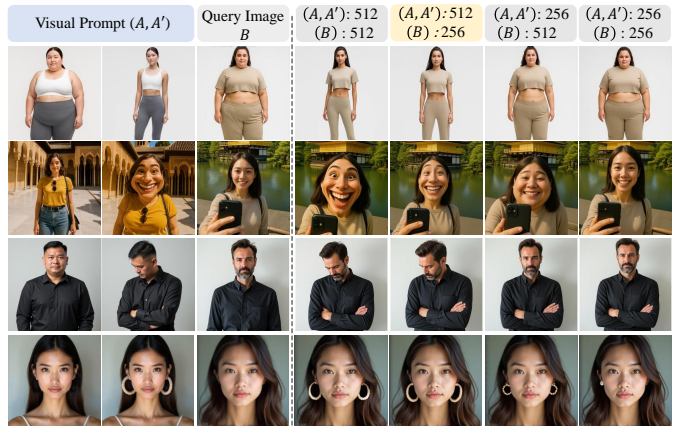


Fig. 12. **Qualitative results under different condition-compression settings.** All outputs are generated at a 1024-pixel long edge. Overly aggressive downsampling (both (A, A') and B at 256) leads to noticeable degradation, whereas using a 512-pixel visual prompt (A, A') and a 256-pixel query image B offers a better trade-off between visual quality and efficiency.

matching the demonstrated transformation. This advantage is reflected in our higher CDS and GPT-A on editing and customization benchmarks, as reported in Table I, as well as by the human preference study in Fig. 11, where our method is consistently preferred for visual-prompt faithfulness.

Consistency. Faithfulness to a visual prompt is not only about producing one correct edit, but also about reproducing the same transformation reliably under different random seeds. To examine this, we randomly sample 100 test cases and generate 5 outputs per case using a shared set of seeds for all methods. As reported in Table I, EditTransfer++ achieves the lowest Var and the highest CLIP-based success rate (SR) across most settings, indicating that it is more robust to sampling randomness while remaining faithful to the visual prompt. Additional qualitative examples in the supplementary material show that, for challenging non-rigid and compositional edits, our outputs are visually more stable across seeds than those of the baselines.

Inference efficiency. Table II reports inference time and peak GPU memory usage when the long side of the generated image is set to 1024 pixels. EditTransfer [9] and VisualCloze [10], which concatenate all image tokens at full resolution, incur the highest computational cost. Although RelationAdapter [11] splits the visual prompt (A, A') and the query–target pair (B, B') into two streams via an adapter, it still runs relatively slowly, and the additional adapter branch increases memory usage at high resolutions. In contrast, EditTransfer++ achieves the fastest inference with a modest memory footprint, benefiting from the proposed condition compression and reuse strategy. This shows that our method not only improves visual-prompt faithfulness, but also offers better practical efficiency for high-resolution edit transfer.

E. Ablation Studies

We conduct an ablation over four proposed components. Starting from the base model M_b trained at a long-edge resolution of 1024 without any of our strategies, we incrementally obtain $M_1 = M_b + \text{TD}$ (text-decoupled training), $M_2 = M_1 + \text{RF}$ (best–worst contrastive refinement), $M_3 = M_2 + \text{DS}$

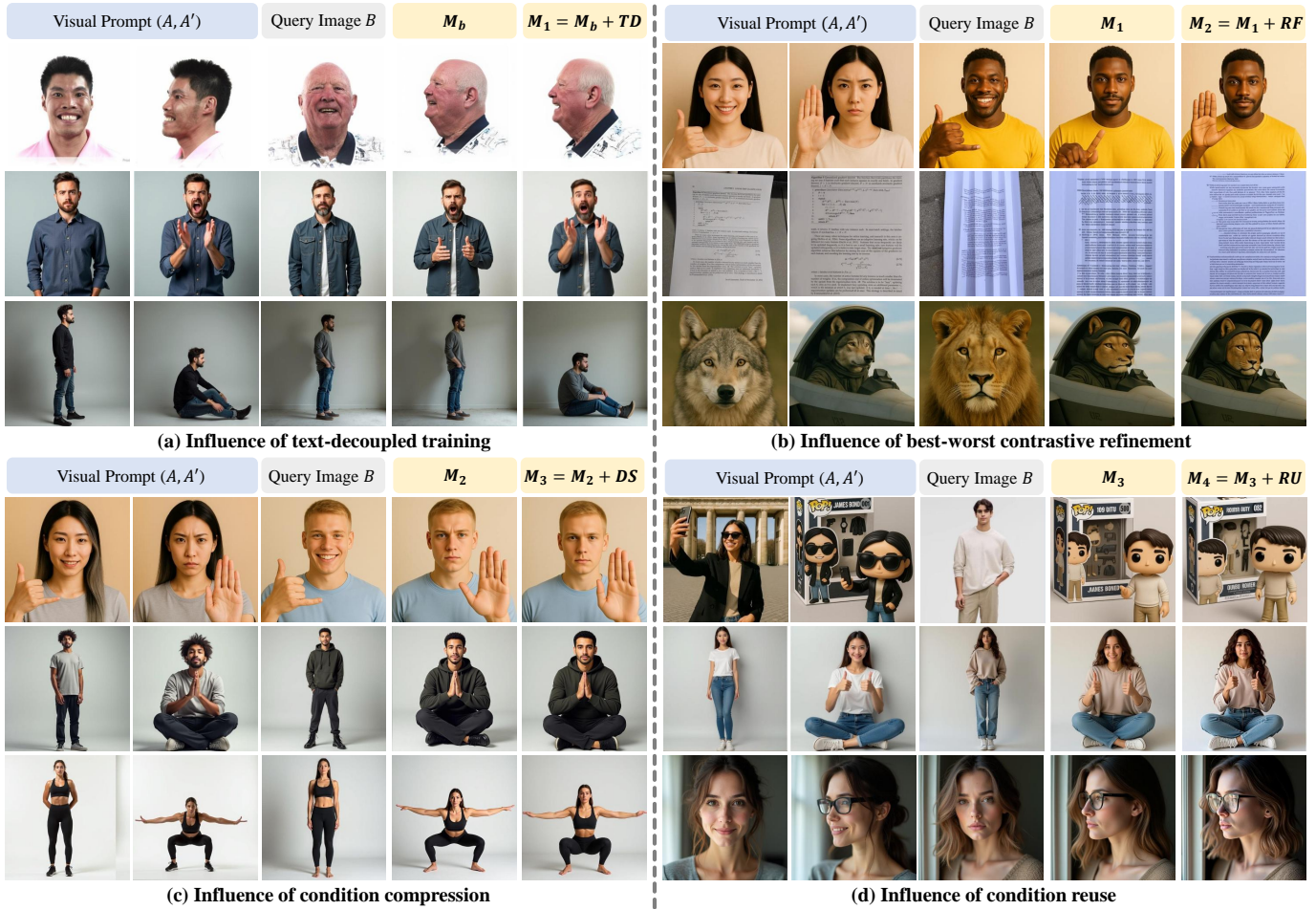


Fig. 13. **Qualitative evaluation of EditTransfer++ components.** (a) Effect of text-decoupled training (TD); (b) effect of best-worst contrastive refinement (RF); (c) effect of condition compression (DS); (d) effect of condition reuse (RU). M_b denotes the base model without our strategies; $M_1 = M_b + TD$, $M_2 = M_1 + DS$, $M_3 = M_2 + RU$, and $M_4 = M_3 + RF$ as the full EditTransfer++ model.

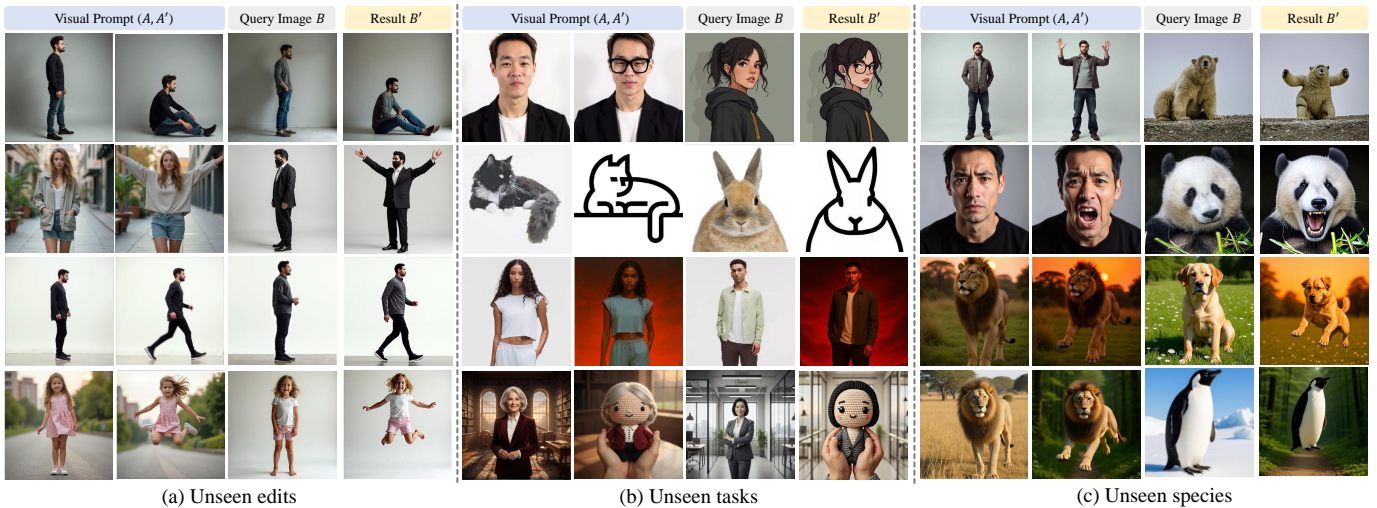


Fig. 14. **Generalization of EditTransfer++.** Qualitative results on (a) unseen edit variants, (b) unseen edit tasks, and (c) unseen species. In all three settings, our method successfully follows the visual prompt for images beyond the training distribution, indicating strong generalization capability.

(condition compression), and $M_4 = M_3 + RU$ (condition reuse), which is the full model.

Impact of text-decoupled training. The text-decoupled strategy plays a critical role in enhancing the faithfulness with the visual prompt. Building on the base model, we train a variant $M_1 = M_b + TD$ using null-text inputs and compare it with the

base model M_b trained with full textual prompts. As shown in Fig. 13(a), although M_b produces reasonable outputs (e.g. the side view edit in the first row) of the Relation252K [11] dataset, it fails to follow the visual prompt on unseen tasks in the second and third rows, exhibiting noticeably weaker alignment to the demonstrated transformations. Quantitative

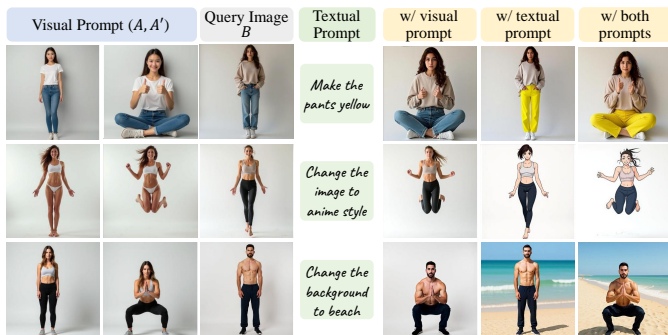


Fig. 15. **Applications of EditTransfer++**. Thanks to text-decoupled training, EditTransfer++ supports visual-prompt-only editing, text-only editing, and combined visual–textual control. This enables flexible compositional edits by conditioning on visual prompts, textual instructions, or their combination.

results in Table III further confirm that applying text-decoupled training in M_1 leads to substantial gains in the CDS, especially on EditTransfer-Bench, demonstrating improved alignment with the visual prompt.

Impact of best-worst contrastive refinement. We compare the outputs of M_2 and $M_1 = M_2 + \text{RF}$, both generated using the same seeds. As shown in Fig. 13(b), incorporating RF effectively corrects previously suboptimal results, reducing visual artifacts and further enhancing faithfulness. For example, in the first row, the gesture produced without RF is incorrect, whereas incorporating RF rectifies the result and aligns it with the visual prompt. Quantitative results in Table III further support these observations, demonstrating improved generation consistency, as reflected by lower variance across samples.

Impact of condition compression and reuse strategy. We first evaluate the efficiency–quality trade-off introduced by the proposed condition compression strategy. Experiments are conducted under five resolution settings, with (A, A') and B downsampled to half (512) or a quarter (256) of the target output, which has a fixed long edge of 1024 pixels. As shown in Fig. 12 and Table IV, aggressively downsampling the visual prompts to 256 greatly reduces inference time but leads to a noticeable loss in faithfulness, as reflected by the clear drop in CDS. In contrast, setting B to 256 and (A, A') to 512 preserves visual alignment, as illustrated in the fifth column of Fig. 12. Therefore, we adopt this configuration and conduct experiments using $M_3 = M_2 + \text{DS}$. As shown in Table III, CDS of M_3 remains comparable, while its variance even exhibits a notable drop. Building on M_3 , the feature reuse strategy is applied to obtain $M_4 = M_3 + \text{RU}$, further reducing inference time. Moreover, this strategy mitigates interference among condition features, yielding cleaner conditioning signals and improved performance, as shown in Fig. 13(d) and Table III.

F. Discussions

Generalization capabilities. As illustrated in Fig. 14, EditTransfer++ exhibits strong generalization ability across several scenarios that are not covered by the training distribution. First, it generalizes to *unseen variants of known edit types*, such as the “sit down” action, whose pose and contact patterns differ significantly from the training samples. Second, it can handle

novel edit types that are absent from the training set, indicating that the model learns transferable editing behaviors rather than memorizing specific instances. Third, it extends to *cross-species edit transfer*, successfully applying transformations demonstrated on one species to visually distinct subjects from another, while preserving their identity and structure.

Roles of text and visual prompts. The text-decoupled training strategy enables *visual-prompt-only* editing, as shown in the fifth column of Fig. 15, where the model follows the demonstrated transformation without relying on textual instructions. At the same time, the underlying T2I backbone retains its *text-only* editing capability, allowing purely language-driven edits when no visual prompt is provided. Moreover, EditTransfer++ naturally supports *joint text–visual* conditioning, where textual and visual prompts are combined to specify the edit, providing flexible and fine-grained compositional control over the final result.

V. CONCLUSIONS

We present **EditTransfer++**, a visual-prompt–guided image editing framework that couples a progressively structured training procedure with an efficient conditioning scheme. The proposed text-decoupled training stage encourages the backbone to learn transformations directly from visual evidence, while the best–worst contrastive refinement stabilizes the denoising trajectories and improves robustness to sampling seeds. For better applicability and scalability, we introduce a condition compression and reuse strategy that reduces token redundancy, enabling high-resolution generation with lower memory usage and computational cost. To assess generalization in the edit transfer setting, we construct **EditTransfer-Bench**, which spans multiple editing types and includes both single- and multi-step edits. Across existing benchmarks and EditTransfer-Bench, EditTransfer++ consistently outperforms prior approaches, delivering more faithful visual-prompt adherence, more stable outputs, and faster inference.

Future work will extend EditTransfer++ to richer multi-condition editing scenarios beyond a single source–target pair and investigate its applicability to broader visual in-context learning tasks.

REFERENCES

- [1] A. Hertz, R. Mokady, J. Tenenbaum, K. Aberman, Y. Pritch, and D. Cohen-Or, “Prompt-to-prompt image editing with cross attention control,” in *ICLR*, 2023.
- [2] M. Cao, X. Wang, Z. Qi, Y. Shan, X. Qie, and Y. Zheng, “Masactrl: Tuning-free mutual self-attention control for consistent image synthesis and editing,” in *ICCV*, 2023.
- [3] T. Brooks, A. Holynski, and A. A. Efros, “Instructpix2pix: Learning to follow image editing instructions,” in *CVPR*, 2023.
- [4] Z. Zhang, J. Xie, Y. Lu, Z. Yang, and Y. Yang, “In-context edit: Enabling instructional image editing with in-context generation in large scale diffusion transformer,” in *NeurIPS*, 2025.
- [5] B. F. Labs, S. Batifol, A. Blattmann, F. Boesel, S. Consul, C. Diagne, T. Dockhorn, J. English, Z. English, P. Esser *et al.*, “Flux. 1 kontext: Flow matching for in-context image generation and editing in latent space,” *arXiv preprint arXiv:2506.15742*, 2025.
- [6] A. Bar, Y. Gandelsman, T. Darrell, A. Globerson, and A. A. Efros, “Visual prompting via image inpainting,” in *NeurIPS*, 2022.
- [7] X. Wang, W. Wang, Y. Cao, C. Shen, and T. Huang, “Images speak in images: A generalist painter for in-context visual learning,” in *CVPR*, 2023.

- [8] Y. Yang, H. Peng, Y. Shen, Y. Yang, H. Hu, L. Qiu, H. Koike *et al.*, “Imagebrush: Learning visual in-context instructions for exemplar-based image manipulation,” in *NeurIPS*, 2023.
- [9] L. Chen, Q. Mao, Y. Gu, and M. Z. Shou, “Edit transfer: Learning image editing via vision in-context relations,” *arXiv preprint arXiv:2503.13327*, 2025.
- [10] Z.-Y. Li, R. Du, J. Yan, L. Zhuo, Z. Li, P. Gao, Z. Ma, and M.-M. Cheng, “Visualcloze: A universal image generation framework via visual in-context learning,” in *ICCV*, 2025.
- [11] Y. Gong, Y. Song, Y. Li, C. Li, and Y. Zhang, “Relationadapter: Learning and transferring visual relation with diffusion transformers,” in *NeurIPS*, 2025.
- [12] H. Lu, J. Chen, Z. Yang, A. T. Gnanha, F. L. Wang, L. Qing, and X. Mao, “Pairedit: Learning semantic variations for exemplar-based image editing,” in *NeurIPS*, 2025.
- [13] Y. Jiang, Y. Gu, Y. Song, I. Tsang, and M. Z. Shou, “Personalized vision via visual in-context learning,” *arXiv preprint arXiv:2509.25172*, 2025.
- [14] W. Peebles and S. Xie, “Scalable diffusion models with transformers,” in *ICCV*, 2023.
- [15] X. Wei, T. Zhang, Y. Li, Y. Zhang, and F. Wu, “Multi-modality cross attention network for image and sentence matching,” in *CVPR*, 2020.
- [16] J. Ho, A. Jain, and P. Abbeel, “Denoising diffusion probabilistic models,” in *NeurIPS*, 2020.
- [17] J. Song, C. Meng, and S. Ermon, “Denoising diffusion implicit models,” in *ICLR*, 2021.
- [18] N. Ruiz, Y. Li, V. Jampani, Y. Pritch, M. Rubinstein, and K. Aberman, “Dreambooth: Fine tuning text-to-image diffusion models for subject-driven generation,” in *CVPR*, 2023.
- [19] Y. Song, S. Huang, C. Yao, H. Ci, X. Ye, J. Liu, Y. Zhang, and M. Z. Shou, “Processpainter: Learning to draw from sequence data,” in *SIGGRAPH Asia*, 2024.
- [20] Y. Zhang, Q. Zhang, Y. Song, J. Zhang, H. Tang, and J. Liu, “Stable-hair: Real-world hair transfer via diffusion model,” in *AAAI*, 2025.
- [21] R. Rombach, A. Blattmann, D. Lorenz, P. Esser, and B. Ommer, “High-resolution image synthesis with latent diffusion models,” in *CVPR*, 2022.
- [22] L. Huang, W. Wang, Z.-F. Wu, Y. Shi, H. Dou, C. Liang, Y. Feng, Y. Liu, and J. Zhou, “In-context lora for diffusion transformers,” *arXiv preprint arXiv:2410.23775*, 2024.
- [23] Z. Tan, S. Liu, X. Yang, Q. Xue, and X. Wang, “Ominicontrol: Minimal and universal control for diffusion transformer,” in *ICCV*, 2024.
- [24] Y. Zhang, Y. Yuan, Y. Song, H. Wang, and J. Liu, “Easycontrol: Adding efficient and flexible control for diffusion transformer,” in *ICCV*, 2025.
- [25] Y. Song, C. Liu, and M. Z. Shou, “Omniconsistency: Learning style-agnostic consistency from paired stylization data,” in *NeurIPS*, 2025.
- [26] Y. Song, C. Liu, and M. Z. Shou, “Makeanything: Harnessing diffusion transformers for multi-domain procedural sequence generation,” *arXiv preprint arXiv:2502.01572*, 2025.
- [27] S. Huang, Y. Song, Y. Zhang, H. Guo, X. Wang, M. Z. Shou, and J. Liu, “Photodoodle: Learning artistic image editing from few-shot pairwise data,” in *ICCV*, 2025.
- [28] J. Wang, J. Pu, Z. Qi, J. Guo, Y. Ma, N. Huang, Y. Chen, X. Li, and Y. Shan, “Taming rectified flow for inversion and editing,” in *ICML*, 2023.
- [29] O. Avrahami, O. Patashnik, O. Fried, E. Nemchinov, K. Aberman, D. Lischinski, and D. Cohen-Or, “Stable flow: Vital layers for training-free image editing,” in *CVPR*, 2025.
- [30] K. Feng, Y. Ma, B. Wang, C. Qi, H. Chen, Q. Chen, and Z. Wang, “Dit4edit: Diffusion transformer for image editing,” in *AAAI*, 2025.
- [31] Y. Feng, J. Li, and M. Zhou, “Instruction-driven multi-weather image translation based on a large-scale image editing model,” *IEEE TIP*, 2025.
- [32] T. Xia, Y. Zhang, T. Liu, and L. Zhang, “Consistent image layout editing with diffusion models,” *IEEE TIP*, 2025.
- [33] K. Zhang, L. Mo, W. Chen, H. Sun, and Y. Su, “Magicbrush: A manually annotated dataset for instruction-guided image editing,” in *NeurIPS*, 2023.
- [34] S. Zhang, X. Yang, Y. Feng, C. Qin, C.-C. Chen, N. Yu, Z. Chen, H. Wang, S. Savarese, S. Ermon *et al.*, “Hive: Harnessing human feedback for instructional visual editing,” in *CVPR*, 2024.
- [35] L. A. Gatys, A. S. Ecker, and M. Bethge, “Image style transfer using convolutional neural networks,” in *CVPR*, 2016.
- [36] Y. Alaluf, D. Garibi, O. Patashnik, H. Averbuch-Elor, and D. Cohen-Or, “Cross-image attention for zero-shot appearance transfer,” in *SIGGRAPH*, 2024.
- [37] J.-Y. Zhu, T. Park, P. Isola, and A. A. Efros, “Unpaired image-to-image translation using cycle-consistent adversarial networks,” in *ICCV*, 2017.
- [38] Y. Zhou, X. Gao, Z. Chen, and H. Huang, “Attention distillation: A unified approach to visual characteristics transfer,” in *CVPR*, 2025.
- [39] Y. Wang, Y. Wei, X. Qian, L. Zhu, and Y. Yang, “Rego: Reference-guided outpainting for scenery image,” *IEEE TIP*, 2024.
- [40] Y. Zhang, Y. Liu, H. Fan, R. Hu, J. Zhang, and Q. Wu, “Consistent image inpainting with pre-perception and cross-perception collaborative processes,” *IEEE Transactions on Image Processing*, 2025.
- [41] X. Chen, L. Huang, Y. Liu, Y. Shen, D. Zhao, and H. Zhao, “Anydoor: Zero-shot object-level image customization,” in *CVPR*, 2024.
- [42] B. Yang, S. Gu, B. Zhang, T. Zhang, X. Chen, X. Sun, D. Chen, and F. Wen, “Paint by example: Exemplar-based image editing with diffusion models,” in *CVPR*, 2023.
- [43] S. Chen and J. Huang, “Specref: A fast training-free baseline of specific reference-condition real image editing,” in *ICICML*, 2023.
- [44] R. He, K. Ma, L. Huang, S. Huang, J. Gao, X. Wei, J. Dai, J. Han, and S. Liu, “Freeddit: Mask-free reference-based image editing with multi-modal instruction,” *IEEE TPAMI*, 2025.
- [45] X. Chen, Y. Feng, M. Chen, Y. Wang, S. Zhang, Y. Liu, Y. Shen, and H. Zhao, “Zero-shot image editing with reference imitation,” in *NeurIPS*, 2025.
- [46] S. D. Biswas, M. Shreve, X. Li, P. Singhal, and K. Roy, “Pixels: Progressive image xemplar-based editing with latent surgery,” in *AAAI*, 2025.
- [47] R. Wu, Y. Yu, F. Zhan, J. Zhang, S. Liao, and S. Lu, “Pocce: Pose-controllable expression editing,” *IEEE TIP*, 2023.
- [48] B. Liu, C. Wang, T. Cao, K. Jia, and J. Huang, “Towards understanding cross and self-attention in stable diffusion for text-guided image editing,” in *CVPR*, 2024.
- [49] Y. Zhang, K. Zhou, and Z. Liu, “What makes good examples for visual in-context learning?” in *NeurIPS*, 2023.
- [50] Y. Liu, X. Chen, X. Ma, X. Wang, J. Zhou, Y. Qiao, and C. Dong, “Unifying image processing as visual prompting question answering,” in *ICML*, 2024.
- [51] X. Wang, W. Wang, Y. Cao, C. Shen, and T. Huang, “Images speak in images: A generalist painter for in-context visual learning,” in *CVPR*, 2023.
- [52] B. F. Labs, “Flux,” 2024. [Online]. Available: <https://github.com/black-forest-labs/flux>
- [53] X. Liu, C. Gong, and Q. Liu, “Flow straight and fast: Learning to generate and transfer data with rectified flow,” in *ICLR*, 2023.
- [54] Y. Lipman, R. T. Chen, H. Ben-Hamu, M. Nickel, and M. Le, “Flow matching for generative modeling,” in *ICLR*, 2023.
- [55] R. Gal, O. Patashnik, H. Maron, A. H. Bermano, G. Chechik, and D. Cohen-Or, “Stylegan-nada: Clip-guided domain adaptation of image generators,” *ACM TOG*, 2022.
- [56] I. Loshchilov and F. Hutter, “Decoupled weight decay regularization,” in *ICLR*, 2019.
- [57] N. Tumanyan, O. Bar-Tal, S. Bagon, and T. Dekel, “Splicing vit features for semantic appearance transfer,” in *CVPR*, 2022.
- [58] OpenAI, “Gpt-4o system card,” 2024. [Online]. Available: <https://arxiv.org/abs/2410.21276>